Title: **Multimode Monitoring of Oxy-gas Combustion through Flame Imaging, Principal Component Analysis and Kernel Support Vector Machine**

Authors: Xiaojing Bai[1],

Gang Lu[2] (Corresponding author),

Md Moinul Hossain[2],

Yong Yan[2, 1,]

Shi Liu[1]

Address: [1.] School of Control and Computer Engineering,

North China Electric Power University,

Beijing, 102206, China

[2.] School of Engineering and Digital Arts,

University of Kent, Canterbury,

Kent CT2 7NT, UK

E -mail: x.bai@ncepu.edu.cn,

g.lu@kent.ac.uk,

m.hossain@kent.ac.uk

y.yan@kent.ac.uk,

liushidr@yahoo.com

Abstract

This paper presents a method for the multimode monitoring of combustion stability under different oxy-gas fired conditions based on flame imaging, principal component analysis and kernel support vector machine (PCA-KSVM) techniques. The images of oxy-gas flames are segmented into premixed and diffused regions through Watershed Transform method. The weighted color and texture features of the diffused and premixed regions are extracted and projected into two subspaces using the PCA to reduce the data dimensions and noises. The multi-class KSVM model is finally built based on the flame features in the principal component subspace to identify the operation condition. Two classic multivariate statistic indices, i.e. Hotelling's T^2 and squared prediction error (SPE), are used to assess the normal and abnormal states for the corresponding operation condition. The experimental results obtained on a lab-scale oxy-gas rig show that the weighted color and texture features of the defined diffused and premixed regions are effective for detecting the combustion state and that the proposed PCA-KSVM model is feasible and effective to monitor a combustion process under variable operation conditions.

Keywords: Combustion stability, Flame imaging, Kernel support vector machine, Principal components analysis, Multimode process monitoring

1. Introduction

The monitoring and diagnostics of combustion stability in combustion systems such as fossil-fuel fired boilers, gas turbines and combustion engines are required to maintain the combustion efficiency, low pollutant emissions and the system safety, particularly under variable operation

conditions (Huang and Yang, 2009; Candel, 2002). This has increasingly become crucial due to the recent trend of using low-quality fuels, fuel blends, biomass and oxy-fuels, which often cause unstable flames and thus many combustion problems including low combustion efficiency and high pollutant emissions (e.g., NO_x, SO_2) (Huang and Yang, 2009). The combustion stability is a broad perception largely related to the quality of flames and depends on many factors including the burner structure, fuel types, air-to-fuel ratio, and the balance between the velocities of flame and the ignitability of fuel, etc. (Huang and Yang, 2009; Sun et al., 2013). Significant effort has been made to develop monitoring and diagnostic techniques to assess the quality of flames theoretically and experimentally and hence the performance of the combustion process (Ballester and García-Armingol, 2010). Among those, soft-computing incorporating flame imaging and image processing techniques have attracted an increasing attention for both laboratorial and industrial applications in recent years.

In general, the imaging and soft-computing based combustion process monitoring has two main steps, i.e., flame imaging and characterization, and the state monitoring (normal or abnormal). Previous studies on flame characterization have laid the foundation for the combustion process monitoring (Qiu et al., 2011; Huang and Zhang, 2008). For example, Qiu et al. (2011) used watershed transformation to segment the regions of interest in coal-fired flame images, which can be very useful for the flame characterization. Huang and Zhang (2008) analyzed the color features of diffused and premixed methane flames based on the RGB (Red, Green and Blue) and HSV (Hue, Saturation, Value) color image models. A combination of flame imaging and soft-computing techniques has also been used for combustion monitoring (González-Cencerrado et al., 2015; Li et al., 2012; Fleury et al., 2013; Chen et al., 2011; Chen et al., 2013; Wang and Ren, 2014; Sun et al., 2015). For example, Li et al. (2012) developed flame image-based burning state recognition systems (i.e., over burning, under burning and normal burning)

of a rotary kiln using heterogeneous features, and fuzzy integral and a segmentation-free approach used for extracting flame features. Wang and Ren (2014) studied the texture features of flame images and developed a generalized learning vector neural network model to monitor the combustion state of a rolling burner. Sun et al. (2013; 2015) suggested a methodology for diagnosing abnormal conditions of the combustion process through direct flame imaging and kernel PCA. A universal index derived from the statistical analysis of flame images was proposed to assess the stability of flame in terms of its color, geometry and luminance. Whilst the above work has proved the feasibility of combining the flame imaging and soft-computing techniques on combustion process monitoring but most of them are considered for detecting the process under an individual operation condition, (i.e., single-mode process). The main problem of the single-mode monitoring methods is that they are based on an assumption that the process is operated under a consistent condition which makes them invalid if the operation changes.

In practice, however, modern combustion systems often operate under variable conditions (i.e., multimode process) so as to meet demands for fuel availability and operation feasibility (Dunia et al., 2012; Van den Kerkhof et al., 2012). The occurrence of such operation changes is part of the normal process behaviors while single-mode monitoring methods are incapable of categorizing these changes. In other word, the existing single-mode monitoring methods have failed to detect abnormal combustion behaviors from normal operation changes under variable conditions. It is therefore the multimode approaches are highly desirable for the combustion stability monitoring and diagnosis under variable operation conditions.

The multimode process monitoring is mainly regarded to identify the process conditions and states (normal or abnormal) under a variety of operation conditions (Qi et al., 2010). Generally,

multimode process monitoring methods are divided into three categories, namely global-models, adaptive-models and local-models. The global models build a uniform model to monitor all the operation conditions (Ma et al., 2012; Song et al., 2014) and in these models, multimode data are transformed into an approximately unimodal or Gaussian distribution using standardization algorithms, and single-model based monitoring methods are then carried out for state monitoring. For example, Ma et al. (2012) developed a local neighborhood standardization strategy based PCA for fault detection in multimode processes. Song et al. (2014) proposed an improved dynamic neighborhood preserving embedding method and combined it with PCA for multimode monitoring. However, it is difficult to consider all operations' changes in one uniform model. Adaptive models, which adjust the monitoring models according to the mode changes, update frequently as the condition changes (Jin et al., 2006; Lee et al., 2006). For example, Jin et al. (2006) proposed a robust recursive PCA modeling procedure to reflect the operating mode change whilst Lee et al. (2006) employed if-then rules for detecting the operation condition changes. However, updating the model parameters depends on experience and process knowledge. Due to the complexity of the combustion process, flame properties do not normally show regular variance among operation conditions. Therefore, the global-model methods and adaptive-models are not suitable for flame image based multimode combustion process monitoring. Finally, local-models identify the operation condition by using clustering methods and detect the state of the corresponding condition (Tong and Yan, 2013). For instance, Chu et al. (2004) proposed a strategy which employed the support vector machine (SVM) and an entropy-based variable selection method for the fault detection and operation mode identification in processes with multimode operations. Zhu et al. (2012) applied k-independent component analysis-principal component analysis (k-ICA-PCA) in the process pattern construction and multimode monitoring. Jiang and Yan (2014) also integrated mutual information-based multi-block PCA, joint probability

and Bayesian inference techniques in the multimode monitoring of a plant-wide process. The proposed schemes were validated through numerical multimode plant-wide example and the Tennessee Eastman benchmark process. However, the main problem in these local models is that the condition identification is usually based on raw data and suffers from the abnormalities and noise of variables. This is the case in the flame imaging based multimode combustion monitoring. The features extracted from the flame images, which are considered as the input variables, suffer from various noises either from the imaging system or combustion process as well as abnormalities. Therefore, it is difficult to determine the most suitable model for every new sample. As a result, the existing local models are not effective for identifying the combustion operations and a new local model based method for combustion process monitoring is desirable.

In this paper, a new flame image characterization method and combination of PCA and kernel SVM (KSVM) techniques are proposed for monitoring the multimode combustion process. This combined method improves the performance of condition identification as compared to KSVM. Image processing algorithms are developed to segment flame images into premixed and diffused regions, the characteristics of which are considered to be highly related to the combustion conditions (such as the fuel type, fuel/air ratio etc.) (Huang and Zhang, 2008). A global PCA model is built to extract the flame features, and the KSVM technique is employed to identify the combustion operation condition. Hotelling's T^2 and SPE statistics (Sun et al., 2013) are then used to assess the state of the condition.

2. Methodology

2.1 General Principle

Fig. 1 shows the technical strategy of the proposed flame imaging and soft-computing based technique for the multimode combustion process monitoring. Flame images are firstly captured using a digital imaging system (refer to section 3.1). The flame region is then extracted after subtracting the background noise using appropriate threshold value (Sun et al., 2013). The extracted flame region is then segmented into 'premixed' and 'diffused' regions using Watershed transform (refer to later section) (Qiu et al., 2011). Consequently, the color and texture features of the premixed and diffused regions are extracted. The flame features in the principal subspace are calculated and used as the dimensionally reduced inputs of the KSVM model. Finally, the PCA-KSVM model is built based on the flame feature vectors to identify the operation conditions. With the use of the PCA-KSVM model, the operation conditions are identified, and the occurrence of abnormal events in different combustion processes are detected by two traditional multiple variable statistics, T^2 and SPE.

2.2 Flame Image Processing

2.2.1 Segmentation of Premixed and Diffused Regions

The segmentation of the premixed and diffused regions from flame images is an essential step for extracting features of the flame. Flames can be premixed, diffused, or somewhere in between depending on the fuel to air ratio (Fristom, 1995). Studies on the flame color have shown that a premixed flame has typically a blue color whilst a diffused flame appears to be a red/orange color, which can be the very effective indicators of the combustion condition and state (Huang and Zhang, 2008). In this study, a segmentation method based on the Watershed transform (Qiu et al., 2011) is used to segment a flame image into the premixed and diffused regions. The Watershed transform is chosen because it has a good response to the weak edges such as flame outer contours (Qiu et al., 2011). In the image processing, the luminous region of the flame image is firstly separated from the background by setting an appropriate threshold

(Sun et al., 2013). Let $\boldsymbol{I}_{RGB}$=[$\boldsymbol{i}_R$, $\boldsymbol{i}_G$, $\boldsymbol{i}_B$] (where $\boldsymbol{i}_R$, $\boldsymbol{i}_G$, $\boldsymbol{i}_B$ are the intensity values of red, green, and blue components of a flame image, respectively) be the complete RGB image of the flame region and a grey–scale flame image $\boldsymbol{I}$, is converted from the $\boldsymbol{I}_{RGB}$ image (ITU-R, 1995).

The diffused region $\boldsymbol{I}_D$, and the premixed region $\boldsymbol{I}_P$, are calculated as follows,

$$\boldsymbol{I}_D(\mu,\nu)=\begin{cases}\boldsymbol{I}_{RGB}(\mu,\nu), & \text{if } WS(\boldsymbol{I})(\mu,\nu)\neq 0 \text{ and } \boldsymbol{i}_R(\mu,\nu)>\boldsymbol{i}_B(\mu,\nu)\\ \text{else } \boldsymbol{I}_D(\mu,\nu)=0\end{cases}, \ (0<\mu\le l,\ 0<\nu\le m)$$

, (1)

$$\boldsymbol{I}_P=\boldsymbol{I}_{RGB}-\boldsymbol{I}_D, \tag{2}$$

where $WS(\cdot)$ is the Watershed transform, l and m are the numbers of image rows and columns, respectively. μ and v are the pixel coordinates, $\mu=1, 2, \cdots, l$, $v=1,2, \cdots, m$.

2.2.2 Feature Extraction

To reduce the noises as well as to ensure that the flame features extracted are representative of flame image characteristics as possible, both the weighted color features and the texture features are extracted from the segmented flame regions. The weighted color features, $F_1 = [f_r, f_g, f_b]$, are composed of the color features of the diffused and premixed regions, and expressed as follows,

$$f_r=\beta\frac{r_P}{r_P+g_P+b_P}+(1-\beta)\frac{r_D}{r_D+g_D+b_D}, \tag{3}$$

$$f_g=\beta\frac{g_P}{r_P+g_P+b_P}+(1-\beta)\frac{g_D}{r_D+g_D+b_D}, \tag{4}$$

$$f_b=\beta\frac{b_P}{r_P+g_P+b_P}+(1-\beta)\frac{b_D}{r_D+g_D+b_D}, \tag{5}$$

where r_P, g_P, b_P, r_D, g_D, b_D represent the mean intensity values of the red, green, and blue components of the premixed and diffused regions, respectively. β is the weight which is the ratio of the area of the premixed region (A_P) and the whole flame area (A_P+A_D) (as shown in Fig. 2), i.e.,

$$\beta = \frac{A_P}{A_P + A_D}. \tag{6}$$

In addition to the color features, the texture features are calculated for the diffused and premixed regions (Haralick et al., 1973). A total of 14 texture features are extracted for each region based on the grey-level co-occurrence matrix, $f_1, f_2, \cdots, f_{14}$, as listed in Table 1. They are a set of numerical parameters related to the flame image inner structure, such as homogeneity, grey-tone linear dependencies, contrast and the complexity. The texture features for diffused and premixed regions are denoted as $\boldsymbol{F}_2 = [f_{D1}, f_{D2}, \cdots, f_{D14}]$, and $\boldsymbol{F}_3 = [f_{P1}, f_{P2}, \cdots, f_{P14}]$. Finally, feature matrix, $\boldsymbol{F}$, is defined as,

$$\boldsymbol{F} = [\boldsymbol{F}_1\ \boldsymbol{F}_2\ \boldsymbol{F}_3]. \tag{7}$$

2.3 PCA-KSVM Model for Combustion Condition Monitoring

2.3.1 Principal Component Analysis and Kernel Support Vector Machine

A. Principal Component Analysis (PCA)

The PCA is a well-established multivariate statistic model which projects standardized data into two orthogonal subspaces so as to reduce the dimensions of the data (Joe Qin, 2003). As it plays an important part in the proposed PCA-KSVM model, a brief introduction is given below for a reader convenience. In general, a PCA model can be described as,

$$\boldsymbol{X} = \boldsymbol{T}\boldsymbol{P}' + \boldsymbol{E}\ , \tag{8}$$

where $\boldsymbol{X}$ is an $M\times N$ matrix of data (M is the number of samples, N is the number of features). $\boldsymbol{T}$ is a score matrix, $\boldsymbol{P}$ is a loading matrix, and $\boldsymbol{E}$ is the matrix of residuals. If the correlation matrix of $\boldsymbol{X}$ is $\boldsymbol{R}$ where $\boldsymbol{R}=\boldsymbol{X}'\boldsymbol{X}/(M-1)$, the singular value decomposition of $\boldsymbol{R}$ can be represented as (Joe Qin, 2003),

$$\boldsymbol{R} = \boldsymbol{U}\boldsymbol{D}\boldsymbol{U}', \tag{9}$$

where $\boldsymbol{U}$ is an $N\times N$ unitary matrix. $\boldsymbol{D}$ is the characteristic value matrix, i.e., $\boldsymbol{D}=diag(\lambda_1, \lambda_2,\cdots, \lambda_N)$, λ is the characteristic value. Letting $\boldsymbol{u}_i$ be an N vector, $\boldsymbol{U}$ can then be described as $\boldsymbol{U}=[\boldsymbol{u}_1, \boldsymbol{u}_2, \cdots, \boldsymbol{u}_N]$. When the number of principal components (PCs) is k, the loading matrix can be expressed as $\boldsymbol{P}=[\boldsymbol{u}_1, \boldsymbol{u}_2, \cdots, \boldsymbol{u}_k]$.

B. Kernel Support Vector Machine

As one of the traditional classifiers, a support vector machine (SVM) model determines the optimal separation hyperplane that can divide the training set into two classes and has widely been used in many applications in the field of mode identification (Chu et al., 2004; Gunn, 1998). For non-linear mapping data, the kernel function, which represents an inner product between samples in a high-dimensional space, is introduced in the SVM model, so called KSVM which is capable of transferring the non-linear data into a separable space. Suppose input training matrix $\{\boldsymbol{x}_i, \boldsymbol{y}_i\}_{i=1}^{M}$ consists input data $x_i \in R^N$ and the corresponding classification result $\boldsymbol{y}_i \in \{-1, +1\}$, a KSVM classifier can be expressed as,

$$y(x) = \mathrm{sgn}[\omega'\phi(x) + b], \tag{10}$$

where $\phi(\cdot)$ is a non-linear mapping function, b is the bias and ω is a weight vector. Kernel function $\Theta(x_i , x_j)= \phi(x_i)'\phi(x_j)$ is used for implicitly mapping the input data into a high-dimensional feature space without knowing the function $\phi(\cdot)$. Therefore, the optimization problem in the KSVM classifier can be expressed as (Gunn, 1998),

$$\arg\min \frac{1}{2} \sum_{i,j=1}^{M} \alpha_i \alpha_j y_i y_j \Theta(x_i, x_j) - \sum_{v=1}^{M} \alpha_v \text{, s.t} \begin{cases} 0 \le \alpha_i \le C, \\ \sum_{i=1}^{l} \alpha_i y_i = 0, \end{cases} \tag{11}$$

where α is the Lagrange multiplier, C is the penalty parameter of the error term. The kernel function used in this study is a 3-degree polynomial function. Let α_i be the optimum solution for the problem, then the non-linear classifier is,

$$y = \text{sgn}\left(\sum_{i=1}^{M} \alpha_i y_i \Theta(x_i, x) + b \right). \tag{12}$$

Although the KSVM is originally designed as a binary classifier, there are three different approaches that address a multi-class problem, i.e., all-together, one-against-all and one-against-one approaches (Sun et al., 2004). The one-against-one method is used in this study because it is faster in training and testing with better recognition rates in comparison to other approaches.

2.3.2 Construction of the PCA-KSVM Model

Fig. 3 is the block diagram of the proposed PCA-KSVM model, where $\boldsymbol{x}_{\tau i}$ ($i=1,2,\ldots, N$) is the vector in the variable matrix $\boldsymbol{X}_\tau$ for the τ^{th} ($\tau=1, 2, \ldots, S$) condition. In the PCA-KSVM, the global PCA model as described in section 2.3.3 is used for the feature selection whilst the multi-classifier contains $S(S-1)/2$ binary KSVMs for total S conditions are built for operation condition identification. Following that, T^2 and SPE statistics are calculated to detect the abnormalities of the corresponding conditions. Details of the method are described as follows.

Step 1: Construction of PCA-KSVM model

To reduce the feature dimensions and identify the operation condition, a global PCA model and a multi-class KSVM model are constructed in this step. If original image feature matrix for

operation condition τ (τ=*1, 2, ..., S*) is noted as $\boldsymbol{X}_\tau$, feature matrix $\boldsymbol{X}$ for total *S* conditions can then be defined as,

$$\boldsymbol{X}= [\boldsymbol{X}_1 \boldsymbol{X}_2 ...\boldsymbol{X}_S]. \tag{12}$$

Unitary matrix $\boldsymbol{U}$ can be calculated according to (9). The loading matrix in the principal subspace, $\boldsymbol{P}_{global}$, can therefore be expressed as,

$$\boldsymbol{P}_{global} = \begin{bmatrix} p_{11} & p_{12} & \cdots & p_{1k} \\ p_{21} & p_{22} & \cdots & p_{2k} \\ \vdots & \vdots & \ddots & \vdots \\ p_{N1} & p_{N2} & \cdots & p_{Nk} \end{bmatrix}. \tag{13}$$

Score matrix in the principal subspace, $\boldsymbol{T}^c = \boldsymbol{X}\boldsymbol{P}_{global}$, is the input of the KSVM and can be calculated as:

$$\boldsymbol{T}^c = \begin{bmatrix} \sum_{i=1}^{N} x_{1i} p_{i1} & \sum_{i=1}^{N} x_{1i} p_{i2} & \cdots & \sum_{i=1}^{N} x_{1i} p_{ik} \\ \sum_{i=1}^{N} x_{2i} p_{i1} & \sum_{i=1}^{N} x_{2i} p_{i2} & \cdots & \sum_{i=1}^{N} x_{2i} p_{ik} \\ \vdots & \vdots & \ddots & \vdots \\ \sum_{i=1}^{N} x_{Mi} p_{i1} & \sum_{i=1}^{N} x_{Mi} p_{i2} & \cdots & \sum_{i=1}^{N} x_{Mi} p_{ik} \end{bmatrix}. \tag{14}$$

Therefore, the KSVM model can be expressed as,

$$y = \mathrm{sgn}[\omega' \phi(T^c) + b]. \tag{15}$$

In the KSVM models, the one-against-one approach, which constructs a binary classifier for every pair of distinct operation conditions, is employed to achieve multi-classification. Therefore, in this study total *S(S-1)/2*=6 binary KSVMs are built for *S=4* conditions. The 'Max-Wins' voting strategy is implemented in these classifiers to determine the final output. The final output of the KSVMs is the operation condition. Details of 'Max-Wins' voting strategy can be found elsewhere in (Sun et al., 2004).

Step 2: Selection of model parameters

The number of principal components, *k,* is the main parameter which determines the performance of the PCA-KSVM model. To ensure that the PCA-KSVM model has a prominent performance, *k* should be selected according to the accuracy of the operation condition identification, i.e. Acc_k, which is expressed as,

$$Acc_k = \left(1 - \frac{1}{M}\sum_{i=1}^{M}(\tau_i - \bar{\tau}_i)\right) \times 100\%, \tag{16}$$

where τ_i represents the identified condition for the i^{th} sample and $\bar{\tau}_i$ is the true condition.

Step 3: Abnormality detection

Once operation condition τ is identified by the PCA-KSVM model, the value of T^2 and SPE are calculated and compared to their control limits to detect abnormalities (Joe Qin, 2003), i.e.,

$$T_\tau^2 = \left\| \boldsymbol{D}_{\tau k}^{-\frac{1}{2}} \boldsymbol{P}_\tau' \boldsymbol{x} \right\|^2 \le \chi_\tau^2, \tag{17}$$

$$\mathrm{SPE}_\tau = \left\| (\boldsymbol{\Xi} - \boldsymbol{P}_\tau \boldsymbol{P}_\tau') \boldsymbol{x} \right\|^2 \le \delta_\tau^2, \tag{18}$$

where $\boldsymbol{\Xi}$ is an identity matrix. $\boldsymbol{D}_\tau$ and $\boldsymbol{P}_\tau$ are the characteristic value matrix and loading matrix for the τ^{th} operation condition. χ_τ^2 and δ_τ^2 are the control limits of T^2 and SPE, respectively. The detailed determination of control limits χ_τ^2 and δ_τ^2 can be found elsewhere (Joe Qin, 2003). The statistics above the control limits means that the process is under an abnormal state, and the deviation of the statistics from the control limits indicates the abnormal level. The statistics under the control limits means that the process is under a normal state.

3. Experimental Results

3.1 Experimental Set-Up

To examine the effectiveness of the proposed PCA-KSVM model for combustion condition and state monitoring, experiments were carried out on a lab-scale oxy-gas combustion test rig under a range of operating conditions. Oxy-fuel combustion is a combustion technology developed to tackle carbon oxide (CO_2) emissions in fossil fuel combustion, where the air is replaced by oxygen and recycled flue gas to oxidize the fuel (Hu et al., 2000). Fig. 4 shows the schematic diagram and the overview of the experimental set-up. Propane was used as the fuel and CO_2 was used to simulate the flue gas. The primary and secondary O_2/CO_2 flows were supplied and mixed with the fuel so that four different combustion conditions are generated. Table 2 summarizes the fuel, O_2, and CO_2 supplies whilst Table 3 gives the summary of the test conditions. In all the test conditions, the equivalent oxygen-fuel ratio (the ratio of actual Air–fuel ratio to stoichiometry for a given mixture. 1.0 is at stoichiometry, <1.0 rich mixtures, and >1.0 lean mixtures) was set to 1.25. The digital imaging system used to capture flame images was previously developed which has mainly an optical probe with a field view of 90° and an industrial RGB (Red, Green and Blue) digital camera with a 1/3 inch imaging sensor of 1280 (h)×1024 (v) pixels at a frame rate of 25 frames per second (Sun et al., 2013). In the experiments, a total of 230 flame images were captured for each test condition in an open and relatively steady environment. The captured 230 images are then categorized into normal and abnormal samples based on statistical analysis of the features in (7). Table 4 summarizes the numbers of the normal and abnormal samples under different test conditions. Note that, due to the complex dynamic nature of the combustion, the transient processes are neglected in the image collection.

3.2 Results and Discussion

The flame images acquired under each test condition were processed, and the premixed and diffused regions of the flame image were segmented using the image segmentation method as

described in Section 2.2. Fig. 5(a) shows the example of 2-D flame images captured under the four test conditions, whilst Fig. 5(b) and (c) show the corresponding segmented premixed and diffused regions. It can clearly be seen that the premixed and diffused regions have different characteristics in nature for the different conditions in terms of the luminous region, luminance level and color composition. In particular, the area of the premixed region decreases and the diffused region (luminosity of the flame) increases with the oxygen supply. It is worth mentioning that the segmentation accuracy is slightly influenced because the boundaries of the diffused and premixed regions are unclear in OF27 and OF30. While the inaccuracy of the features caused by the segmenting errors can be reduced by employing PCA in process monitoring.

The mean value of the weighted color features for the four test conditions are illustrated in Fig. 6. The standard deviations of the mean value of the weighted color are also indicated as error bars in the figure. As can be seen, the mean values of f_r and f_g increase and f_b decreases with the oxygen level, indicating that the dominated region of the flame has changed from 'premixed' to 'diffused'. In addition, the maximum standard deviation is 0.4% observed at operating condition OF30, which suggests that the weighted color features extracted are stable and reliable. The results illustrate that the weighted color features represent well the information of premixed and diffused regions. The texture features of 230 flame images (each condition) is calculated from grey-level co-occurrence matrix, which have numerical means about the texture characteristics of the flame images. The averages of the texture features for the premixed and diffused regions under different operations are summarized in Table 5 and Table 6, respectively. It is clear that the most texture features extracted from the flame images, especially the diffused region, exhibit a close relationship with the operation condition. Both

the weighted color and the texture features are then used as inputs to train the PCA-KSVM model.

In the training stage, a total of 640 flame images for four operation conditions (160 for each condition) were processed and the features were used as the training data. To determine the number of k and ensure the performance of the PCA-KSVM model, the identification accuracy of the conditions [refer to Eq. (16)] was assessed under different numbers of principal components (PCs). 10-fold cross validation is employed for selecting the optimal number of k (Kohavi, 1995) and ensured that the selected number of PCs is robust for different samples. In the 10-fold cross validation, the training set is firstly divided into 10 groups randomly with the equal number of image samples (i.e., 64 images in each group). 9 out of 10 groups are used to train the PCA-KSVM model and the remained group is to test the trained model. The identification accuracy of the different number of PCs is calculated using the equation (16) and the condition identification accuracy is shown in Fig. 7. It is clear that the accuracy increases rapidly with the number of PCs and reaches 99.7% when the number of PCs is 6. The accuracy decreases undulately when the number of PCs is 7 or over because the increased principal components may introduce more noise and abnormalities. In this study, an irregular trend has been observed for the identification accuracy due to the complexity of the flame image features and lack of training data. But it still conforms to the expected trend of this case. Based on this assessment, the optimal number of PCs, $k = 6$ is set for test stage in this study.

Once the PCA-KSVM model is trained, flame images, which contain both normal and abnormal samples under different combustion conditions, were used to evaluate the performance of the proposed PCA-KSVM. A total of 280 images (70 flame images for each condition) were processed and their features were extracted for the testing purpose. The result

of the output is composed of two parts, i.e. the operation condition identification and the state recognition. The condition identification is firstly detected and the process state (normal or abnormal) is then determined for the corresponding operation condition.

Fig. 8 illustrates the results of the condition identification and it can clearly be seen that the trained PCA-KSVM method successfully identified the change of the operation conditions. The accuracy of the proposed method for the condition identification is more than 99% even when some abnormalities occur. In order to evaluate the effectiveness of the PCA-KSVM, the performance of the PCA-KSVM is compared with that of the KSVM and the results are shown in Fig. 8. It shows that there are more false identifications of KSVM compared to the PCA-KSVM. Table 7 shows the identification accuracy of PCA-KSVM and KSVM. As can be seen, the identification accuracy increases with oxygen level for both PCA-KSVM and KSVM. It is attributed to that the diffused region increases while the differences of the diffused region are more significant than the premixed region for different conditions. Besides, it is obvious that the PCA-KSVM outperformed the KSVM in terms of the condition identification accuracy. This is mainly due to the fact that, in the PCA-KSVM, the interference of the noise and abnormalities is removed by the PCA. The results have shown that the combination of the PCA and KSVM can effectively reduce the adverse effect of noise and abnormalities in the operation condition identification.

Fig. 9(a) and (b) show the results of the state monitoring for the corresponding operation condition. As can be seen from Fig. 9, T^2 and SPE control limits vary for different operation conditions due to the fact that flame features extracted vary with the conditions and thus the control limits must be adjusted to reflect such changes. It is clear that, for the normal samples, computed T^2 and SPE statistics are below the control limits, while for the abnormal samples,

either T^2 or SPE statistics is above the control limits. It can therefore be concluded that the proposed process monitoring method can recognize abnormal states when they occur in each condition.

It should, however, be noted that there are some missed detections of abnormalities in the results. This may be because that the training data in this experiment is limited and can be improved by increasing the number of training data. In addition, the PCA-KSVM is a data driven modeling approach, therefore flame data for all objective operation conditions should be used to train the PCA-KSVM model. It should also be mentioned that, in this study, the flame images were captured on the lab-scale combustion rig – the flame has distinct premixed and diffused regions. In large-scale burners, however, flames may not exhibit obvious distinctions in color due to the fuel type, burner structure, air/fuel ratio, etc. In such cases, the algorithms may have to be improved by taking into considerations different flame features, particularly the color features as inputs to the PCA-KSVM model.

4. Conclusions

This paper presents a novel flame imaging and PCA-KSVM based process monitoring method to monitor the state of oxy-gas combustion under multiple operation conditions. By employing the Watershed transform, the flame images are segmented into diffused and premixed regions. The weighted color and texture features are extracted as the inputs of the proposed PCA-KSVM model. In the PCA-KSVM model, the PCA and KSVM are combined to identify the combustion operation condition and the Hotelling's T^2 and SPE statistics have been used to determine the process state. The experimental results on a lab-scale oxy-gas combustion test rig have demonstrated that the weighted color and texture features extracted using the proposed

image processing algorithms are capable of representing the characteristics of the flame. Furthermore, the results have also shown that the PCA-KSVM outperforms the KSVM in identifying the operation condition. The method proposed is effective in detecting the combustion state in multimode processes.

Acknowledgments

The authors wish to acknowledge the Chinese Ministry of Science and Technology (MOST) , the Chinese Ministry of Education and the Fundamental Research Funds for the Central Universities (No.2014XS42) for providing financial support for this research as part of the 973 Project (2012CB215203) and part of the 111 Talent Introduction Projects (B13009) at North China Electric Power University.

References

Ballester, J. and García-Armingol, T. 2010. Diagnostic techniques for the monitoring and control of practical flames. *Prog. Energy Combust. Sci.,* **36***,* 375-411.

Candel, S. 2002. Combustion dynamics and control: Progress and challenges. *Proc. Combust. Inst.,* **29***,* 1-28.

Chen, J., Chan, L. L. T. and Cheng, Y. C. 2013. Gaussian process regression based optimal design of combustion systems using flame images. *Appl. Energy,* **111***,* 153-160.

Chen, J., Hsu, T. Y., Chen, C. C. and Cheng, Y. C. 2011. Online predictive monitoring using dynamic imaging of furnaces with the combinational method of multiway principal component analysis and hidden Markov model. *Ind. Eng. Chem. Res.,* **50***,* 2946-2958.

Chu, Y. H., Qin, S. J. and Han, C. 2004. Fault detection and operation mode identification based on pattern classification with variable selection. *Ind. Eng. Chem. Res.,* **43***,* 1701-1710.

Dunia, R., Edgar, T. F., Blevins, T. and Wojsznis, W. 2012. Multistate analytics for continuous processes. *J. Process Control,* **22***,* 1445-1456.

Fleury, A. T., Trigo, F. C. and Martins, F. P. R. 2013. A new approach based on computer vision and non-linear Kalman filtering to monitor the nebulization quality of oil flames. *Expert Syst. Appl.,* **40***,* 4760-4769.

Fristom, R. M. 1995. *Flame structure and processes.* New York: Oxford University Press, pp. 19-29.

González-Cencerrado, A., Peña, B. and Gil, A. 2015. Experimental analysis of biomass co-firing flames in a pulverized fuel swirl burner using a CCD based visualization system. *Fuel Process. Technol.,* **130***,* 299-310.

Gunn, S. R. 1998. Support vector machines for classification and regression. ISIS Technical Report, May 10, University of Southampton.

Haralick, R. M., Shanmugam, K. and Dinstein, I. H. 1973. Textural features for image classification. *IEEE Trans. Syst., Man Cybern.,* **6***,* 610-621.

Hu, Y., Naito, S., Kobayashi, N. and Hasatani, M. 2000. CO2, NOx and SO2 emissions from the combustion of coal with high oxygen concentration gases. *Fuel,* **79***,* 1925-1932.

Huang, H. W. and Zhang, Y. 2008. Flame colour characterization in the visible and infrared spectrum using a digital camera and image processing. *Meas. Sci. Technol.,* **19***,* 085406.

Huang, Y. and Yang, V. 2009. Dynamics and stability of lean-premixed swirl-stabilized combustion. *Prog. Energy Combust. Sci.,* **35***,* 293-364.

ITU-R, Recommendation. 1995. BT 601: Studio encoding parameters of digital television for standard 4: 3 and wide-screen 16: 9 aspect ratios. ITU, Geneva, Switzerland.

Jiang, Q. and Yan, X. 2014. Monitoring multi-mode plant-wide processes by using mutual information-based multi-block PCA, joint probability, and Bayesian inference. *Chemometr. Intell. Lab.,* **136***,* 121-137.

Jin, H. D., Lee, Y. H., Lee, G. and Han, C. 2006. Robust recursive principal component analysis modeling for adaptive monitoring. *Ind. Eng. Chem. Res.,* **45***,* 696-703.

Joe Qin, S. 2003. Statistical process monitoring: basics and beyond. *J. Chemom.,* **17***,* 480-502.

Kohavi, R. 1995. A study of cross-validation and bootstrap for accuracy estimation and model selection. *In: 14th International Joint Conference on Artificial Intelligence (IJCAI)*, August 20-25, Montréal Québec, Canada. San Francisco, CA, USA: Morgan Kaufmann Publishers Inc., pp. 1137-1145.

Lee, Y. H., Jin, H. D. and Han, C. 2006. On-line process state classification for adaptive monitoring. *Ind. Eng. Chem. Res.,* **45***,* 3095-3107.

Li, W., Wang, D. and Chai, T. 2012. Flame image-based burning state recognition for sintering process of rotary kiln using heterogeneous features and fuzzy integral. *IEEE Trans. Ind. Inf.,* **8***,* 780-790.

Ma, H., Hu, Y. and Shi, H. 2012. A novel local neighborhood standardization strategy and its application in fault detection of multimode processes. *Chemometr. Intell. Lab.,* **118***,* 287-300.

Qi, Y., Wang, P., Chen, X. and Gao, X. 2010. A novel stage-based multiple PCA monitoring approach for batch processes. *In: 2010 International Conference on Computational and Information Sciences (ICCIS)*, December 17-19, Chengdu, China. IEEE, pp. 45-49. Available at: http://dx.doi.org/ 10.1109/ICCIS.2010.18.

Qiu, T., Yan, Y. and Lu, G. 2011. Watershed transformation based identification of the combustion region in an oxy-coal flame image. In: *2011 Sixth International Conference on*

Image and Graphics (ICIG), August 12-15 Hefei, Anhui, China. IEEE, pp. 152-156. Available at: http://dx.doi.org/10.1109/ICIG.2011.175.

Song, B., Ma, Y. and Shi, H. 2014. Multimode process monitoring using improved dynamic neighborhood preserving embedding. *Chemometr. Intell. Lab.,* **135***,* 17-30.

Sun, D., Lu, G., Zhou, H. and Yan, Y. 2013. Condition monitoring of combustion processes through flame imaging and kernel principal component analysis. *Combust. Sci. Technol.,* **185***,* 1400-1413.

Sun, D., Lu, G., Zhou, H., Yan, Y. and Liu, S. 2015. Quantitative assessment of flame stability through image processing and spectral analysis. *IEEE Trans. Instrum. Meas.,* **64***,* 3323-3333.

Sun, J., Rahman, M., Wong, Y. and Hong, G. 2004. Multiclassification of tool wear with support vector machine by manufacturing loss consideration. *Int. J. Mach. Tools Manuf.,* **44***,* 1179-1187.

Tong, C. and Yan, X. 2013. Double monitoring of common and specific features for multimode process. *Asia Pac. J. Chem. Eng.,* **8***,* 730-741.

Van den Kerkhof, P., Gins, G., Vanlaer, J. and Van Impe, J. F. M. 2012. Dynamic model-based fault diagnosis for (bio) chemical batch processes. *Comput. Chem. Eng.,* **40***,* 12-21.

Wang, J. and Ren, X. 2014. GLCM based extraction of flame image texture features and KPCA-GLVQ recognition method for rotary kiln combustion working conditions. *Int. J. Autom. Comput.,* **11***,* 72-77.

Zhu, Z., Song, Z. and Palazoglu, A. 2012. Process pattern construction and multi-mode monitoring. *J. Process Control,* **22***,* 247-262.

List of Figures

List of Tables

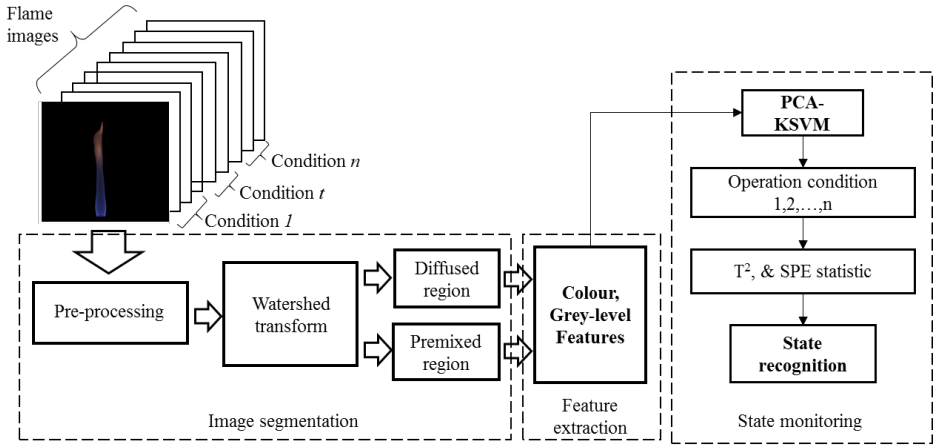

Fig.1 Technical strategy for multimode monitoring of oxy-gas combustion through flame image processing and PCA-KSVM.

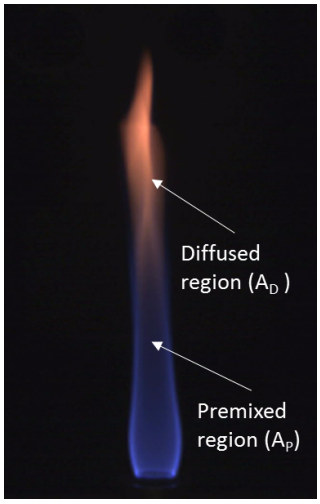

Fig. 2 A typical flame image with diffused and premixed regions.

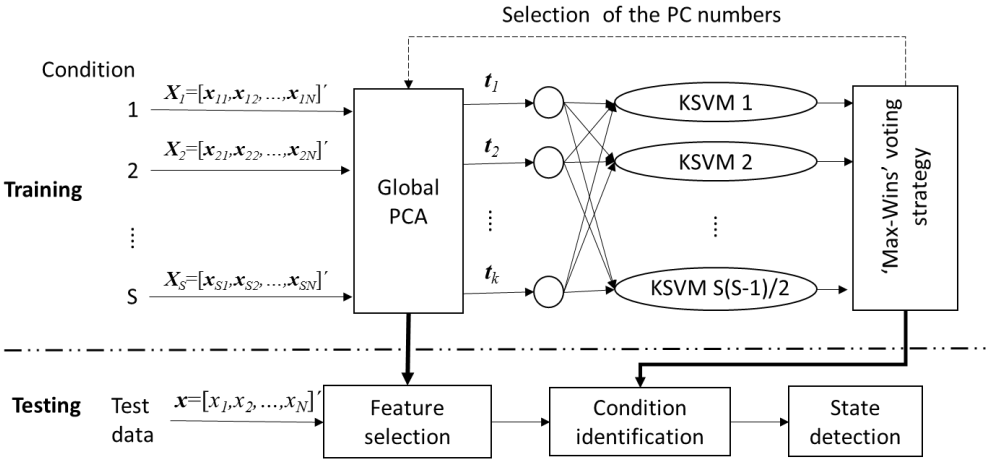

Fig. 3 Block diagram of the PCA-KSVM model.

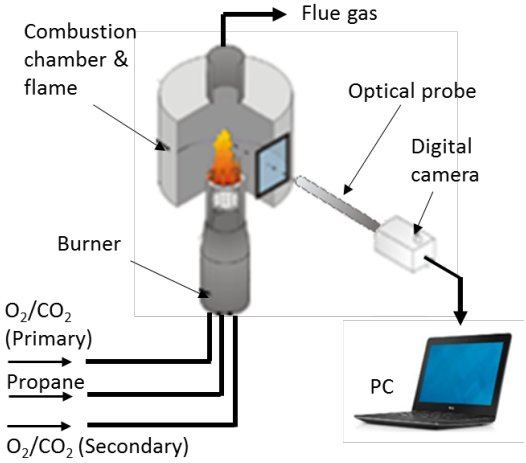

(a) Schematic of the system.

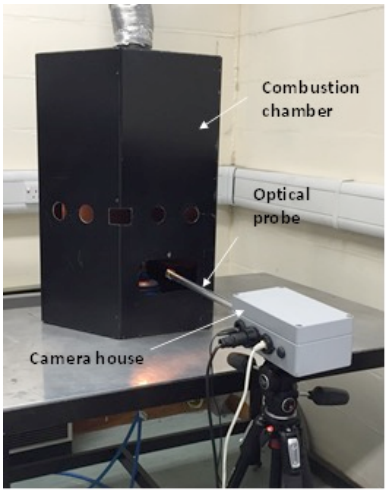

(b) Photo of the set-up.

Fig. 4 Experimental set-up.

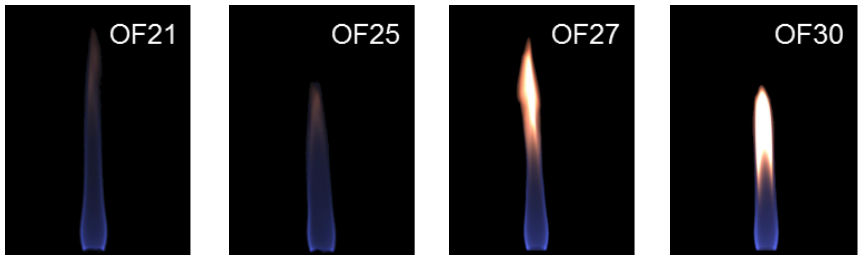

(a) Flame images under the four test conditions.

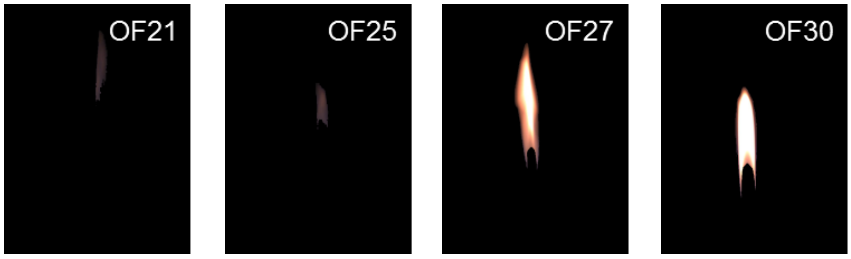

(b) Segmented diffused region for the flame images (a).

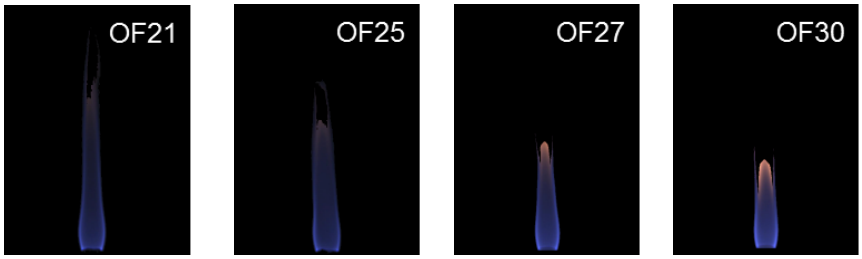

(c) Segmented premixed region for the flame images (a).

Fig. 5 Flame images and their segmented premixed and diffused regions under four experimental conditions.

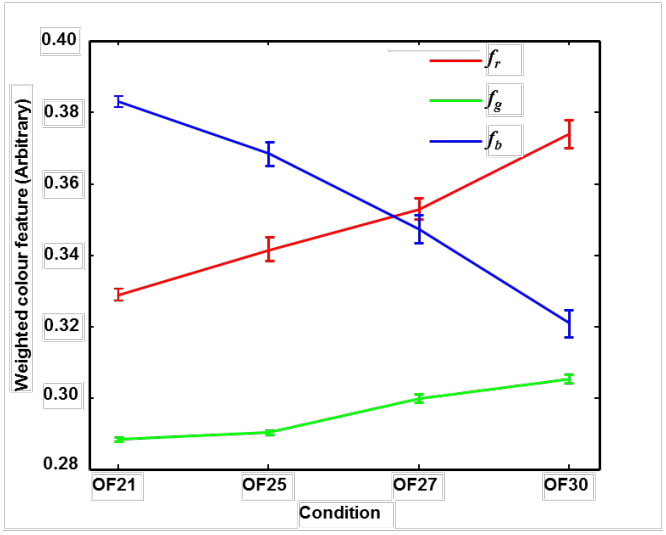

Fig. 6 Weighted color features for four test conditions.

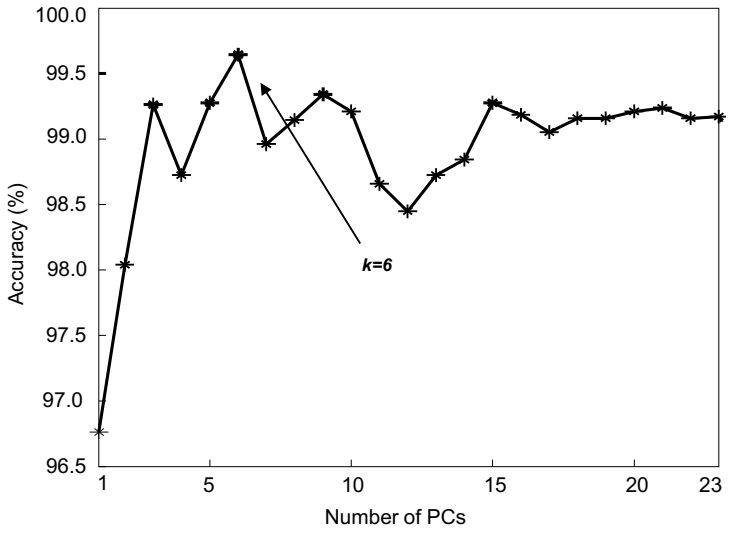

Fig. 7 Accuracy of the condition identification for the different number of principal components.

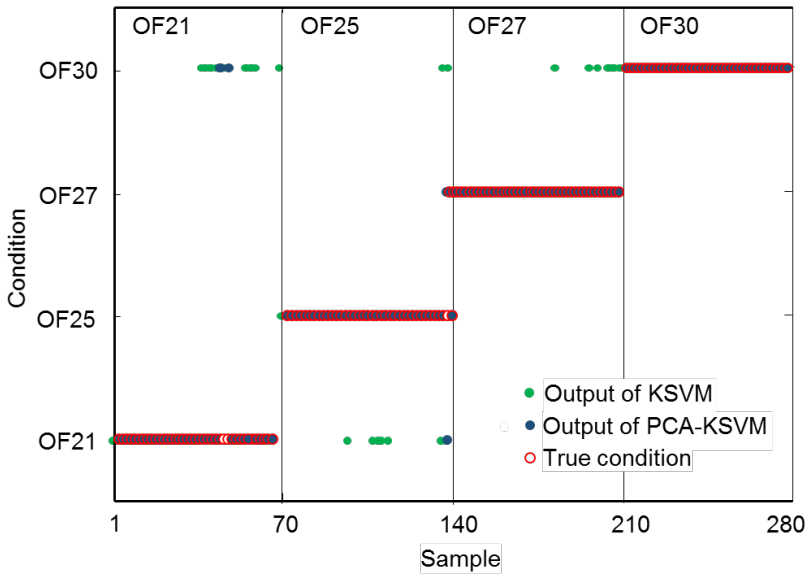

Fig. 8 Results of condition identification by the PCA-KSVM and KSVM in the test stage.

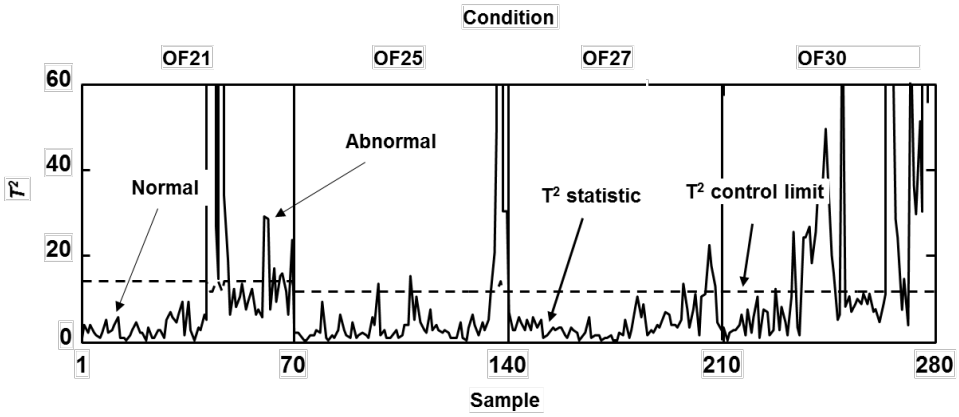

(a) T^2 statistic.

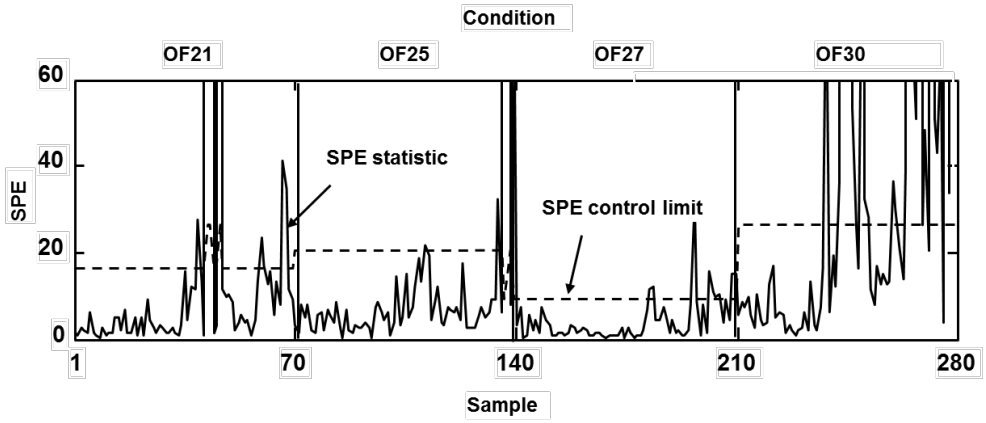

(b) SPE statistic.

Fig. 9 Results of the state monitoring.

Table 1. List of texture features.

	Texture features		Texture features
f_1	angular second moment	f_8	sum entropy
f_2	contrast	f_9	entropy
f_3	correlation	f_{10}	difference variance
f_4	sum of squares	f_{11}	difference entropy
f_5	inverse difference moment	f_{12}-f_{13}	information measures of correlation
f_6	sum average		
f_7	sum variance	f_{14}	maximum correlation coefficient

Table 2. Summary of fuel/O_2/CO_2 supplies.

Fuel/O_2/CO_2 supply	Value
Propane (C_3H_8)	0.014 *g/s*
Oxygen (O_2)	0.064 *g/s*
Primary O_2 + CO_2	15% of O_2 + CO_2
Secondary O_2 + CO_2	85% of O_2 + CO_2

Table 3. Summary of the test conditions.

Test condition	Volume (%)		Mass (%)	
	O_2	CO_2	O_2	CO_2
OF21	21	79	16.20	83.80
OF25	25	75	19.51	80.49
OF27	27	73	21.20	78.80
OF30	30	70	23.76	76.24

Table 4. Test samples under different test conditions.

Test condition	Normal samples	Abnormal samples
OF21	1-190	191-230
OF25	1-219	220-230
OF17	1-225	226-230
OF30	1-210	211-230

Table 5. Texture features for the premixed region ($x10^{-2}$).

Features	f_1	f_2	f_3	f_4	F_5	f_6	f_7	f_8	f_9	f_{10}	f_{11}	f_{12}	f_{13}	f_{14}
OF21	0.852	0.007	0.989	0.725	0.999	2.312	5.096	0.358	0.363	0.062	0.018	-0.962	0.700	0.921
OF25	0.857	0.011	0.988	0.929	0.999	2.370	5.948	0.342	0.344	0.062	0.013	-0.973	0.692	0.924
OF27	0.995	0.032	0.796	0.104	0.999	2.023	4.284	0.023	0.024	0.062	0.007	-0.758	0.170	0.998
OF30	0.996	0.070	0.789	0.199	0.999	2.031	4.632	0.021	0.022	0.062	0.007	-0.767	0.164	0.998

Table 6. Texture features for the diffused region.

Features	f_1	f_2	f_3	f_4	F_5	f_6	f_7	f_8	f_9	f_{10}	f_{11}	f_{12}	f_{13}	f_{14}
OF21	0.916	0.007	0.979	0.360	0.999	2.155	4.330	0.230	0.234	0.062	0.020	-0.929	0.578	0.957
OF25	0.855	0.013	0.996	2.453	0.998	2.637	11.414	0.432	0.436	0.062	0.029	-0.948	0.738	0.924
OF27	0.743	0.041	0.998	11.473	0.995	3.878	44.087	0.753	0.761	0.061	0.057	-0.941	0.861	0.861
OF30	0.763	0.076	0.996	12.479	0.996	3.905	48.778	0.659	0.665	0.062	0.045	-0.949	0.836	0.872

Table 7. Comparison between the identification accuracies of PCA-KSVM and KSVM.

Operation condition identification accuracy	Condition			
	OF21	OF25	OF27	OF30
PCA-KSVM (%)	99.4	99.5	100.0	100.0
KSVM (%)	78.5	87.1	90.0	100.0